

Ultra Wideband Microwave Ten-Port Reflectometer

Amirhossein Askarian¹ and Gholamreza Moradi²

¹ Department of Electrical Engineering
Graduate Student of Amirkabir University of Technology, Tehran, Iran
askarian.amirhossein@aut.ac.ir

² Department of Electrical Engineering
Associate Professor of Amirkabir University of Technology, Tehran, Iran
ghmoradi@aut.ac.ir

Abstract — This paper describes and simulates the Ultra Wideband (UWB) Ten-Port Reflectometer (TPR). It is based on the concept of well-known six-port structure so that numbers of measuring ports are increased to eight in order to improve reliability and accuracy as well. This article presents UWB (2 GHz to 12 GHz) reflectometer using Rectangular Waveguide (RWG). It is proved that increasing numbers of measuring ports leads to improving accuracy and reliability of structure so that each port with corresponding port help to make wideband reflectometer as well as having reliable and robust structure. This prototype of ten-port reflectometer is simulated by Agilent ADS and using RWG that has more bandwidth, less loss and high Q-factor than other common transmission lines, say microstrip, SIW and CPW.

Index Terms — CPW, DUT, q-point, RWG, SIW, SPR, UWB, VNA.

I. INTRODUCTION

A six-port measurement technique (first introduced by Engen in 1977 [1]) is a simple and low cost method for measuring complex reflection coefficient in respect to conventional method using Vector Network Analyzer (VNA) [1]. Six-Port Reflectometer (SPR) is formed by a passive circuit with four scalar power detector ports for measuring the power and two ports for connecting the microwave source and Device Under Test (DUT). Very various structures for SPR proposed and analyzed in recent years, the SPRs have minimum-requirement numbers of ports for determining of

complex reflection coefficient so that incapacitating of one power detector makes ambiguity in calculating of reflection coefficient. Key of solving this problem is increasing the numbers of measuring ports. In this paper we have increased them up to eight so that each measuring port has the back-up port. With counting two ports for signal generator and DUT mentioned structure has ten ports. In other words, simple ten-port reflectometer consisting of a structure with two ports for signal input and output and eight measuring ports with their corresponding power detectors for sampling the standing wave within the transmission line [2,3].

Figure 1 depicts the general diagram of TPR with planar structure, it consisting of two power dividers and nine 3 dB directional couplers that connected together via specified-length transmission lines. Lengths of transmission lines have been calculated in order to obtain maximum accuracy and precision for determining reflection coefficient when frequency is changed between microwave frequencies of 2 GHz and 12 GHz [1]. General equation of the TPR is presented in equation (1), which consists of six circles so that intersection of them in complex plane, obtain the unique complex reflection coefficient [1-3]:

$$p_i = k_i |\Gamma - q_i|^2 \quad i = 1, 2, \dots, 6, \quad (1)$$

where p_i is normalized power in each measuring port, k_i is calibration constant, Γ is complex reflection coefficient of DUT and q_i is circles center that depend on the TPR structure.

In ideal frequency-compensation TPR, when frequency is changed, characteristic (say S-

parameters) of the reflectometer must not be changed because intersection of circles should be in specified point, which only depends on the reflection coefficient of DUT. In practice, however, centers of circles q_i -points rotate in Γ plane with wide variety of frequency. As mentioned in equation (1), six equations in TPR with corresponding six q_i -points arranged symmetrically around the plane as shown in Fig. 2, in other words,

phase of three q_i -points, q_1 , q_2 , and q_3 differ by about 120 degrees and about q_4 , q_5 , and q_6 as well. These two groups are arranged with 180 degrees out-of-phase in Γ plane. In other words, mentioned TPR consists of two six-port structures that coupled together by means of two 3 dB directional couplers 1 and 2 according to Fig. 2. Mentioned couplers make 180 degrees out-of-phase in each group of q_i -points.

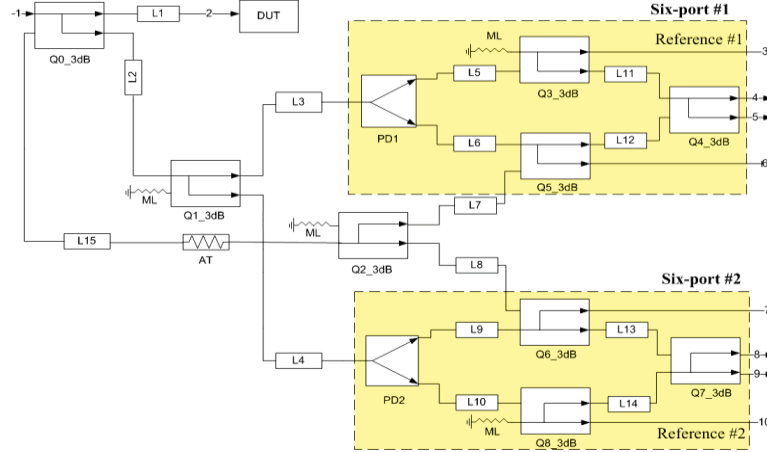


Fig. 1. General diagram of TPR.

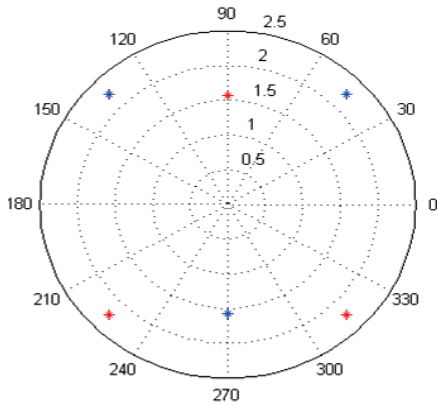


Fig. 2. Constellation of q_i -points in TPR.

II. ANALYSIS OF FREQUENCY-COMPENSATION OF TPR

In the design undertaken here, the chosen component are two power dividers, nine 3 dB directional couplers, one 3 dB attenuator and fifteen specified-length RWGs between components, with schematic shown in Fig. 1. Optimum length of transmission lines help improve accuracy. In order to analyze and determine the proper physical length of mentioned transmission lines in the TPR,

assuming that all ports between components are matched or reflected wave from unmatched ports are passed up. θ_i , θ_p and θ_q are electrical length of transmission lines, power dividers and directional couplers respectively, $1/\alpha$ (where $|\alpha| > 1$) is attenuation of the attenuator in linear scale and b_i ($i=3,4\dots 10$) is detected wave in i^{th} port of TPR, a_1 is incident wave to first port (reference wave), b_2 and a_2 are incident and reflected waves from DUT respectively, so that desirable reflection coefficient is $\Gamma = a_2/b_2$. Incident wave of DUT expressed in equation (2):

$$a_1 = \sqrt{2}b_2e^{j(\theta_1+\theta_2)}. \quad (2)$$

Incident wave to each measuring port are:

$$b_3 = -\frac{1}{4}a_1e^{-j(3\theta_q+\theta_2+\theta_3+\theta_p+\theta_5)}, \quad (3)$$

$$b_4 = \frac{a_1}{4\sqrt{2}} \left(je^{-j(4\theta_q+\theta_2+\theta_3+\theta_p+\theta_5+\theta_{11})} - e^{-j(4\theta_q+\theta_2+\theta_3+\theta_p+\theta_6+\theta_{12})} \right) - \frac{ja_2}{4\alpha} e^{-j(4\theta_q+\theta_1+\theta_{15}+\theta_7+\theta_{12})}, \quad (4)$$

$$b_5 = \frac{a_1}{4\sqrt{2}} \left(je^{-j(4\theta_q+\theta_2+\theta_3+\theta_p+\theta_6+\theta_{12})} - e^{-j(4\theta_q+\theta_2+\theta_3+\theta_p+\theta_5+\theta_{11})} \right) - \frac{a_2}{4\alpha} e^{-j(4\theta_q+\theta_1+\theta_{15}+\theta_7+\theta_{12})}, \quad (5)$$

$$b_6 = -\frac{a_1}{4} e^{-j(3\theta_q + \theta_2 + \theta_3 + \theta_p + \theta_6)} + j \frac{a_2}{2\sqrt{2}\alpha} e^{-j(\theta_1 + \theta_{15} + 3\theta_q + \theta_7)}, \quad (6)$$

$$b_7 = -j \frac{a_1}{4} e^{-j(3\theta_q + \theta_2 + \theta_4 + \theta_p + \theta_9)} + \frac{a_2}{2\sqrt{2}\alpha} e^{-j(\theta_1 + \theta_{15} + 3\theta_q + \theta_8)}, \quad (7)$$

$$b_8 = \frac{-a_1}{4\sqrt{2}} (j e^{-j(4\theta_q + \theta_2 + \theta_4 + \theta_p + \theta_{10} + \theta_{14})} + e^{-j(4\theta_q + \theta_2 + \theta_4 + \theta_p + \theta_9 + \theta_{13})}) + \frac{j a_2}{4\sqrt{2}\alpha} e^{-j(5\theta_q + \theta_1 + \theta_{15} + \theta_8 + \theta_{13})}, \quad (8)$$

$$b_9 = \frac{-a_1}{4\sqrt{2}} (e^{-j(4\theta_q + \theta_2 + \theta_4 + \theta_p + \theta_9 + \theta_{13})} + e^{-j(4\theta_q + \theta_2 + \theta_4 + \theta_p + \theta_{10} + \theta_{14})}) - \frac{a_2}{4\sqrt{2}\alpha} e^{-j(5\theta_q + \theta_1 + \theta_{15} + \theta_8 + \theta_{13})}, \quad (9)$$

$$b_{10} = -j \frac{a_1}{4} e^{-j(3\theta_q + \theta_2 + \theta_4 + \theta_p + \theta_{10})}. \quad (10)$$

With substituting a_1 from equation (2) into equations (3) to (10), and remember that $P_i = |b_i|^2$, detected powers to each port are:

$$P_3 = |b_3|^2 = \frac{|b_2|^2}{8}, \quad (11)$$

$$P_4 = |b_4|^2 = \frac{|b_2|^2}{16\alpha^2} |\Gamma - \alpha(e^{-j(-\theta_q - 2\theta_1 - \theta_{15} - \theta_7 - \theta_{12} + \theta_2 + \theta_3 + \theta_p + \theta_5 + \theta_{11})} + j e^{-j(-\theta_q - 2\theta_1 - \theta_{15} - \theta_7 + \theta_2 + \theta_3 + \theta_p + \theta_6)})|^2, \quad (12)$$

$$P_5 = |b_5|^2 = \frac{|b_2|^2}{16\alpha^2} |\Gamma - \alpha(-e^{-j(-\theta_q - 2\theta_1 - \theta_{15} - \theta_7 - \theta_{12} + \theta_2 + \theta_3 + \theta_p + \theta_5 + \theta_{11})} + j e^{-j(-\theta_q - 2\theta_1 - \theta_{15} - \theta_7 + \theta_2 + \theta_3 + \theta_p + \theta_6)})|^2, \quad (13)$$

$$P_6 = |b_6|^2 = \frac{|b_2|^2}{8\alpha^2} |\Gamma - j\alpha(-e^{-j(-\theta_q - 2\theta_1 + \theta_2 + \theta_3 + \theta_p + \theta_6 - \theta_{15} - \theta_7)})|^2, \quad (14)$$

$$P_7 = |b_7|^2 = \frac{|b_2|^2}{8\alpha^2} |\Gamma - j\alpha(e^{-j(-\theta_q - 2\theta_1 + \theta_2 + \theta_4 + \theta_p + \theta_9 - \theta_{15} - \theta_8)})|^2, \quad (15)$$

$$P_8 = |b_8|^2 = \frac{|b_2|^2}{32\alpha^2} |\Gamma - \alpha\sqrt{2}(-j e^{-j(-2\theta_q - 2\theta_1 - \theta_{15} - \theta_8 + \theta_2 + \theta_4 + \theta_p + \theta_9)} + e^{-j(-2\theta_q - 2\theta_1 - \theta_{15} - \theta_8 - \theta_{13} + \theta_2 + \theta_4 + \theta_p + \theta_{10} + \theta_{14})})|^2, \quad (16)$$

$$P_9 = |b_9|^2 = \frac{|b_2|^2}{32\alpha^2} |\Gamma - \alpha\sqrt{2}(-j e^{-j(-2\theta_q - 2\theta_1 - \theta_{15} - \theta_8 + \theta_2 + \theta_4 + \theta_p + \theta_9)} - e^{-j(-2\theta_q - 2\theta_1 - \theta_{15} - \theta_8 - \theta_{13} + \theta_2 + \theta_4 + \theta_p + \theta_{10} + \theta_{14})})|^2, \quad (17)$$

$$P_{10} = |b_{10}|^2 = \frac{|b_2|^2}{8}, \quad (18)$$

where P_3 and P_{10} are reference ports (in this paper have been used to analyze according to reference port [1]). Whereas, in the general case, incident power to DUT is unknown parameter so it can be

eliminated by normalizing equations (12) to (17) by referencing ports (equations (11) and (18)). Since ports 3 and 10 are only response to incident wave, so there are two reference ports in presented TPR. Thus, P_4 , P_5 , and P_6 are normalized by P_3 and P_7 , P_8 and P_9 are normalized by P_{10} . The resulting six circles equations, therefore, in accordance with equation (1) are:

$$p_4 = \frac{1}{2\alpha^2} |\Gamma - \alpha(e^{-j(-\theta_q - 2\theta_1 - \theta_{15} - \theta_7 - \theta_{12} + \theta_2 + \theta_3 + \theta_p + \theta_5 + \theta_{11})} + j e^{-j(-\theta_q - 2\theta_1 - \theta_{15} - \theta_7 + \theta_2 + \theta_3 + \theta_p + \theta_6)})|^2, \quad (19)$$

$$p_5 = \frac{1}{2\alpha^2} |\Gamma - \alpha(-e^{-j(-\theta_q - 2\theta_1 - \theta_{15} - \theta_7 - \theta_{12} + \theta_2 + \theta_3 + \theta_p + \theta_5 + \theta_{11})} + j e^{-j(-\theta_q - 2\theta_1 - \theta_{15} - \theta_7 + \theta_2 + \theta_3 + \theta_p + \theta_6)})|^2, \quad (20)$$

$$p_6 = \frac{1}{\alpha^2} |\Gamma - \alpha(-j e^{-j(-\theta_q - 2\theta_1 + \theta_2 + \theta_3 + \theta_p + \theta_6 - \theta_{15} - \theta_7)})|^2, \quad (21)$$

$$p_7 = \frac{1}{\alpha^2} |\Gamma - \alpha(j e^{-j(-\theta_q - 2\theta_1 + \theta_2 + \theta_4 + \theta_p + \theta_9 - \theta_{15} - \theta_8)})|^2, \quad (22)$$

$$p_8 = \frac{1}{4\alpha^2} |\Gamma - \alpha\sqrt{2}(-j e^{-j(-2\theta_q - 2\theta_1 - \theta_{15} - \theta_8 + \theta_2 + \theta_4 + \theta_p + \theta_9)} + e^{-j(-2\theta_q - 2\theta_1 - \theta_{15} - \theta_8 - \theta_{13} + \theta_2 + \theta_4 + \theta_p + \theta_{10} + \theta_{14})})|^2, \quad (23)$$

$$p_9 = \frac{1}{4\alpha^2} |\Gamma - \alpha\sqrt{2}(-j e^{-j(-2\theta_q - 2\theta_1 - \theta_{15} - \theta_8 + \theta_2 + \theta_4 + \theta_p + \theta_9)} - e^{-j(-2\theta_q - 2\theta_1 - \theta_{15} - \theta_8 - \theta_{13} + \theta_2 + \theta_4 + \theta_p + \theta_{10} + \theta_{14})})|^2, \quad (24)$$

Solving six equations (19) to (24) obtain desirable Γ . Graphically, intersection of these six circles will be in one point in Γ plan ($|\Gamma| < 1$). Thus, far centers of circles are:

$$q_4 = \alpha(e^{-j(-\theta_q - 2\theta_1 - \theta_{15} - \theta_7 - \theta_{12} + \theta_2 + \theta_3 + \theta_p + \theta_5 + \theta_{11})} + j e^{-j(-\theta_q - 2\theta_1 - \theta_{15} - \theta_7 + \theta_2 + \theta_3 + \theta_p + \theta_6)}), \quad (25)$$

$$q_5 = \alpha(-e^{-j(-\theta_q - 2\theta_1 - \theta_{15} - \theta_7 - \theta_{12} + \theta_2 + \theta_3 + \theta_p + \theta_5 + \theta_{11})} + j e^{-j(-\theta_q - 2\theta_1 - \theta_{15} - \theta_7 + \theta_2 + \theta_3 + \theta_p + \theta_6)}), \quad (26)$$

$$q_6 = j\alpha(-e^{-j(-\theta_q - 2\theta_1 + \theta_2 + \theta_3 + \theta_p + \theta_6 - \theta_{15} - \theta_7)}), \quad (27)$$

$$q_7 = j\alpha(e^{-j(-\theta_q - 2\theta_1 + \theta_2 + \theta_4 + \theta_p + \theta_9 - \theta_{15} - \theta_8)}), \quad (28)$$

$$q_8 = \alpha\sqrt{2}(-e^{-j(-2\theta_q - 2\theta_1 - \theta_{15} - \theta_8 + \theta_2 + \theta_4 + \theta_p + \theta_9)} - j e^{-j(-2\theta_q - 2\theta_1 - \theta_{15} - \theta_8 - \theta_{13} + \theta_2 + \theta_4 + \theta_p + \theta_{10} + \theta_{14})}), \quad (29)$$

$$q_9 = \alpha\sqrt{2}(-e^{-j(-2\theta_q - 2\theta_1 - \theta_{15} - \theta_8 + \theta_2 + \theta_4 + \theta_p + \theta_9)} + j e^{-j(-2\theta_q - 2\theta_1 - \theta_{15} - \theta_8 - \theta_{13} + \theta_2 + \theta_4 + \theta_p + \theta_{10} + \theta_{14})}), \quad (30)$$

For $\theta = \beta l$ and $\beta = 2\pi/\lambda$ (TEM wave), when frequency is changed, centers of circles rotate in Γ plan; hence, additional transmission lines θ_i help to dump rotation and improve the accuracy of system where of q_i -points are in constant place by means of solving equation (31):

$$\begin{cases} -\theta_q - 2\theta_1 - \theta_{15} - \theta_7 - \theta_{12} + \theta_2 + \theta_3 + \theta_p + \theta_5 + \theta_{11} = 0 \\ -\theta_q - 2\theta_1 - \theta_{15} - \theta_7 + \theta_2 + \theta_3 + \theta_p + \theta_6 = 0 \\ -\theta_q - 2\theta_1 + \theta_2 + \theta_3 + \theta_p + \theta_6 - \theta_{15} - \theta_7 = 0 \\ -\theta_q - 2\theta_1 + \theta_2 + \theta_4 + \theta_p + \theta_9 - \theta_{15} - \theta_8 = 0 \\ -2\theta_q - 2\theta_1 - \theta_{15} - \theta_8 + \theta_2 + \theta_4 + \theta_p + \theta_9 = 0 \\ -2\theta_q - 2\theta_1 - \theta_{15} - \theta_8 - \theta_{13} + \theta_2 + \theta_4 + \theta_p + \theta_{10} + \theta_{14} = 0 \end{cases} \quad (31)$$

So optimum lengths of transmission lines for frequency-compensate TPR are obtained. After satisfying equation (31), centers of circles that are shown in Fig. 2 are:

$$q_4 = \alpha(1 + j) = \alpha\sqrt{2}e^{j\frac{\pi}{4}}, \quad (32)$$

$$q_5 = \alpha(-1 + j) = \alpha\sqrt{2}e^{j\frac{3\pi}{4}}, \quad (33)$$

$$q_6 = -j\alpha = \alpha e^{-j\frac{\pi}{2}}, \quad (34)$$

$$q_7 = j\alpha = \alpha e^{j\frac{\pi}{2}}, \quad (35)$$

$$q_8 = \alpha\sqrt{2}(1 - j) = 2\alpha e^{j\frac{7\pi}{4}}, \quad (36)$$

$$q_9 = \alpha\sqrt{2}(-1 - j) = 2\alpha e^{j\frac{5\pi}{4}}. \quad (37)$$

Another optimization is carried out with simulation to this structure in Agilent ADS software, by means of RWG as transmission lines. In this case we have used some blocks entitled power divider (three-port block) and directional couplers (four-port block), then we have applied specific S-parameters for each block and added RWG to each port of blocks for satisfying electrical length property of them with specific electrical length according to equation (41). If the general equation of TPR is considered according to equation (38) [1]:

$$r_i^2 = |\Gamma - Q_i|^2 \quad i = 4, 5, \dots, 9, \quad (38)$$

where r_i and Q_i are according to equations (39) and (40) [1]:

$$\begin{cases} Q_i = \frac{\frac{p_i}{q_3} \frac{\mu_i^2}{|q_3|^2} q_i}{\frac{p_i}{|q_3|^2} \frac{\mu_i^2}{|q_3|^2}} & i = 4, 5, 6 \\ Q_i = \frac{\frac{p_i}{q_{10}} \frac{\mu_i^2}{|q_{10}|^2} q_i}{\frac{p_i}{|q_{10}|^2} \frac{\mu_i^2}{|q_{10}|^2}} & i = 7, 8, 9 \end{cases}, \quad (39)$$

$$\begin{cases} r_i^2 = \frac{p_i \left| \frac{\mu_i}{q_3} + \frac{q_i \mu_i}{|q_3|^2} \right|^2}{\left| \frac{\mu_i^2}{|q_3|^2} \frac{p_i}{|q_3|^2} \right|^2} & i = 4, 5, 6 \\ r_i^2 = \frac{p_i \left| \frac{\mu_i}{q_{10}} + \frac{q_i \mu_i}{|q_{10}|^2} \right|^2}{\left| \frac{\mu_i^2}{|q_{10}|^2} \frac{p_i}{|q_{10}|^2} \right|^2} & i = 7, 8, 9 \end{cases}, \quad (40)$$

where $p_i = P_i/P_3$, $\mu_i = h_i/h_3$ for $i=4, 5, 6$ and $p_i = P_i/P_{10}$, $\mu_i = h_i/h_{10}$ for $i=7, 8, 9$, and

$$\begin{aligned} h_i &= (s_{i2}s_{21} - s_{22}s_{i1})/s_{21} \quad \text{for } i = 4, 5, \dots, 9, \\ q_i &= s_{i1}/(s_{22}s_{i1} - s_{i2}s_{21}) \quad \text{for } i = 4, 5, \dots, 9. \end{aligned}$$

Important point is that, with selection electrical length of transmission lines in center frequency according to equation (41), two groups of q_i -points (q_4, q_5, q_6 and q_7, q_8, q_9) corresponding to two six-port structures, have different behaviours consistent with frequency variations. Figure 4 shows phase change of Q_i -points in TPR structures in 2 GHz to 12 GHz frequency range with employment of equation (41):

$$\begin{aligned} \theta_1 &= \theta_p = \theta_q = 2.25^\circ, \\ \theta_9 &= \theta_6 = \theta_3 = \theta_{15} = 3.2^\circ, \\ \theta_{13} &= \theta_2 = \theta_{12} = \theta_{11} = \theta_{14} = 2.25^\circ, \\ \theta_4 &= 3.6 \times \theta_3, \\ \theta_5 &= 1.2 \times \theta_q, \\ \theta_7 &= \theta_8 = 4.7^\circ, \\ \theta_{10} &= 1.2 \times \theta_5, \\ \text{AT} &= 3 \text{ dB}, \\ a_{rec} &= 3000 \text{ mils}, \quad b_{rec} = 1500 \text{ mils}, \end{aligned} \quad (41)$$

where θ_i is electrical length of RWG, AT is attenuation of attenuator that changes magnitude of q_i -points (according to equation (32) to (37)), a_{rec} and b_{rec} are width and height of RWG respectively. Figure 3 shows intersections of six mentioned circles in equations (39) and (40), with transmission lines according to equation (41) for a sample DUT. As Fig. 2 shows, the magnitudes of q_i -points are about $1.5 \leq |Q_i| \leq 2.5$ so the approximated dynamic range required for power meters given by [2]:

$$\text{Dynamic range [dB]} = 20 \log_{10} \left[\frac{|Q_i| + 1}{|Q_i| - 1} \right]. \quad (42)$$

Dynamic range is 7.36 dB corresponding to $|Q_i|=2.5$ and 14 dB corresponding to $|Q_i|=1.5$.

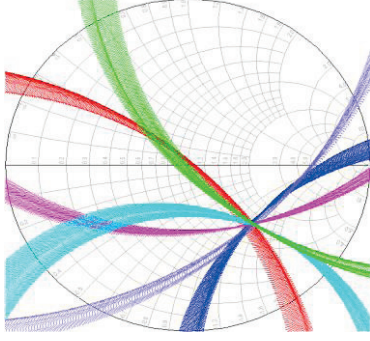


Fig. 3. Intersection of six circles in TPR for a sample DUT $0.5 < -45^\circ$; thicknesses of lines indicate frequency variations of q_i -points.

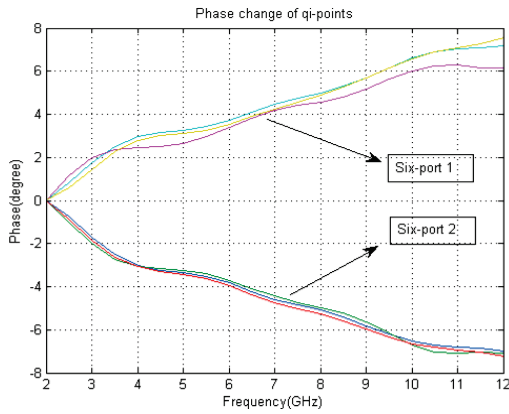


Fig. 4. Phase change of Q_i -points.

A. Improving accuracy of TPR by new q_i -points

As Fig. 4 depicts, phase of Q_i -points in each group are changed in opposite direction (and changed about 8 degrees from 2 GHz to 12 GHz), in other words, three Q_i -points are rotated in clockwise and three remained Q_i -points are rotated in counter clockwise. So this property can be used for eliminating of frequency-dependent property of Q_i -points. Since each group of Q_i -points has 180 degrees out-of-phase, so with defining new three q_i' -points in accordance with equation (40):

$$\begin{aligned} q_1' &= \frac{Q_4 - Q_5}{2}, \\ q_2' &= \frac{Q_6 - Q_7}{2}, \\ q_3' &= \frac{Q_8 - Q_9}{2}, \\ q_4' &= \frac{Q_5 - Q_4}{2}, \\ q_5' &= \frac{Q_7 - Q_6}{2}, \\ q_6' &= \frac{Q_9 - Q_8}{2}. \end{aligned} \quad (43)$$

Figure 5 shows change in the phase of new

centers (equation (40)), so new centers are fixing in Γ plan with wide variety frequency sweep. Table 1 shows magnitudes and phases of new q_i' -points.

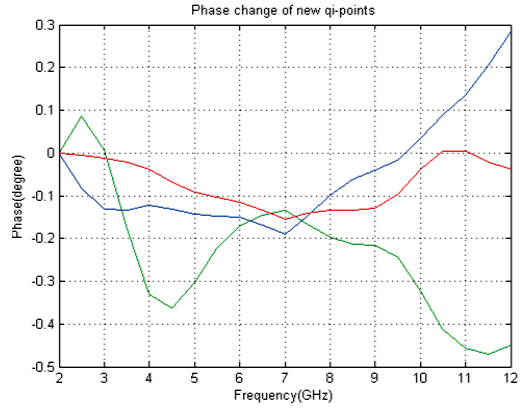


Fig. 5. Phase change of q_i' -points.

Table 1: Magnitudes and phases of q_i' -points

Frequency [GHz]	q_1' (or $-q_4'$) Mag/Phase	q_2' (or q_5') Mag/Phase	q_3' (or $-q_6'$) Mag/Phase
2	2.08/-135.246	1.415/89.926	1.980/-45.185
3	2.005/-135.113	1.413/89.939	1.979/-45.190
4	2.001/-135.122	1.413/89.965	1.985/-44.855
5	1.995/-135.103	1.411/90.017	1.996/-44.883
6	1.992/-135.095	1.410/90.042	1.997/-45.014
7	1.988/-135.057	1.409/90.082	1.997/-45.050
8	1.987/-135.146	1.408/90.059	1.996/-44.988
9	1.984/-135.205	1.408/90.056	1.995/-44.969
10	1.981/-135.280	1.408/89.964	1.992/-44.861
11	1.979/-135.382	1.404/89.923	1.992/-44.729
12	1.975/-135.531	1.403/89.966	1.996/-44.736

B. Calculating of reflection coefficient

As mentioned, in TPR intersection of six circles obtain unique point in complex plan that is reflection coefficient. Since at least three circles are needed, and of course, enough for determining one unique point in plan, six circles in calculating reflection coefficient give more assurance in TPR. On the other hand, with utilization of equation (43), calculating of reflection coefficient is carried out with more precision since new six q_i' -points are approximately frequency-independent. For evaluating operation of mentioned TPR, results of simulation for sample DUT $\Gamma=0.5 < -45^\circ$, in Agilent ADS exported to Matlab to solve equation (38) and obtain the Γ by numerical methods, calculated magnitude and phase of reflection coefficient Γ is plotted in Figs. 6 and 7 respectively. This simulation is performed by two group q_i -points that

are introduced in equations (39) and (43). The result shows that calculated phase of reflection coefficient in wide frequency range based on equation (43), is more accurate than equation (39). Figures 8 and 9 respectively, show magnitude and phase error rate for calculating reflection coefficient $\Gamma=0.5/-45^\circ$ in TPR. As shown, maximum deviation in calculating of phase and magnitude is 2.8% and 1.8% respectively when using equation (43), but the values are 7% and 1.7% with utilizing equation (39). So this kind of TPR can be very useful in applications that need to precise phase detector (that can be used in radar systems or microwave image systems, whereas, in the image processing technique, maximum information of image is concealment in the phase [5,6,8]) to work in ultra wide frequency range.

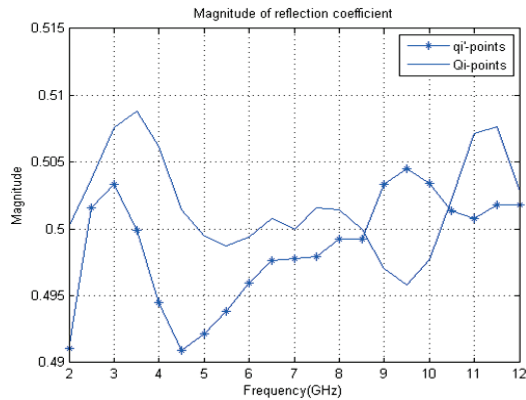


Fig. 6. Magnitude of reflection coefficient with utilizing q_i' -points (equation (43)) and Q_i -points (equation (39)) when frequency is changed between 2 GHz to 12 GHz.

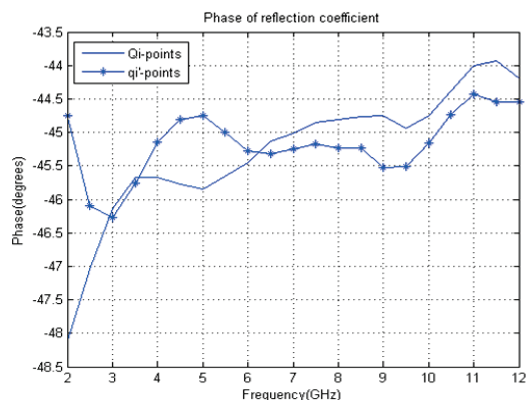


Fig. 7. Phase of reflection coefficient with utilizing q_i' -points (equation (43)) and Q_i -points (equation (39)) when frequency is changed between 2 GHz to 12 GHz.

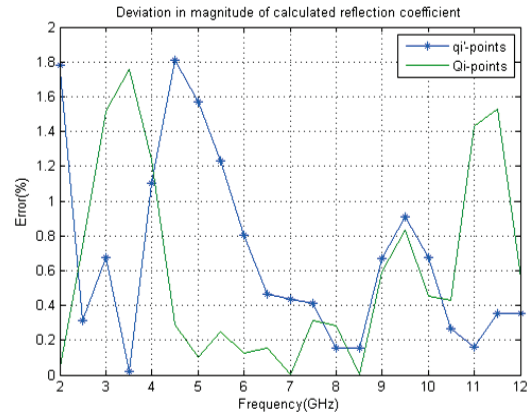


Fig. 8. Deviation in magnitude of reflection coefficient.

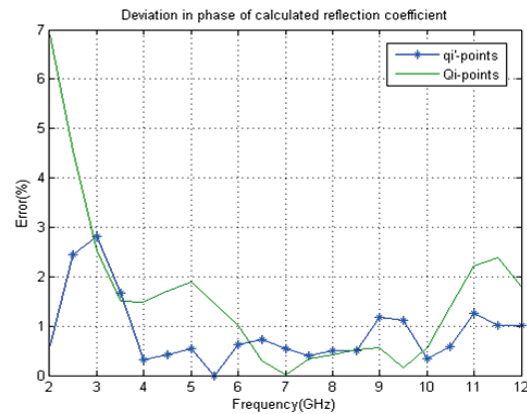


Fig. 9. Deviation in phase of reflection coefficient.

C. Optimum attenuation for attenuator

In Prototype ten-port reflectometer investigated by RWG, Ports 1 and 2 are connected to signal generator and DUT respectively. The reflected wave from DUT passes through a 3 dB attenuator in order to push away q_i -points from unit circle. By adding a 3 dB attenuator in the reflection route, Q_i -points positioned in the Γ plane push away from the center of smith chart so optimum case $1.5 < |Q_i| < 2.5$ can be chosen by equation (42) and following items. Magnitude of q_i -points should be greater than one; it should not be too near to unity because P_i (measured power) could be small for the fully reflecting terminations. Small values of P_i resulting from $|Q_i| \cong 1$ decrease the measurement accuracy. On the other hand, if $|Q_i|$ is too large, it can be seen that a small change to P_i represents a large changing Γ . Therefore, postulated that magnitude of Q_i -points should be in the range of about $\sqrt{2}$ to 2 [4].

III. CONCLUSION

In this paper a prototype of UWB ten-port reflectometer by means of RWG is designed, analyzed and simulated by Agilent ADS and Matlab softwares. Ten-port reflectometer is a proper, robust, accurate and reliable structure for calculating Γ by employing eight ports for power measuring and two ports for input and output signal. In this prototype, required dynamic range for each power detector is between 7.36 dB and 14 dB that depends on frequency change of q_i -points. Increasing number of ports up to ten is a good solution, whereas, system becomes robust and reliable as well as more accurate for important goals such as radar and microwave imaging systems [9-11]. In this paper, new method for increasing phase detection of DUT is presented according to ten-port properties. On the other hand, this structure helps to improve accuracy of system so that mentioned TPR has about 50% relative bandwidth with proper precision. One of outstanding advantage of this article, is designing and simulating by means of RWG, whereas, SIW technology is very similar to RWG in structure, propagation modes and etc. Also, SIW is a planer structure, low-cost, small size with simplicity of integration and easy to manufacture rather than RWG [7,12]. Therefore, SIW is a good candidate for RWG structure and then these results will be valid for SIW structure.

REFERENCES

- [1] F. M. Ghannouchi and A. Mohammadi, "The six-port technique with microwave and wireless application," *Artech House*, September 30, 2009.
- [2] V. Zhurbenka, "Advanced microwave circuits and systems," *InTech*, April 2010.
- [3] J. L. Pedreno-Molina, J. Monzo-Cabrera, A. Lozano-Guerrero, and A. Toledo-Moreo, "Design and validation of a ten-port waveguide reflectometer sensor: application to efficiency measurement and optimization of microwave-heating ovens," *Sensors* 2008, 8, 7833-7849; DOI: 10.3390/s127833.
- [4] J. Monzo-Cabrera, J. L. Pedreno-Molina, A. Lozano-Guerrero, and A. Toledo-Moreo, "A novel design of a robust ten-port microwave reflectometer with autonomous calibration by using neural network," *IEEE Transaction on Microwave Theory and Techniques*, vol. 56, no. 12, December 2008.
- [5] M. Traii, M. Nedil, A. Gharsallah, and T. A. Denidni, "Design of a six-port junction based on single layer technology for UWB application," *In Electrical and Computer Engineering (CCECE), 2010, 23rd Canadian Conference*, pp. 1-4, Tunisia, 2010.
- [6] M. E. Bialkowski, N. Seman, and W. C. Khor, "Design of a six-port reflectometer for a microwave breast cancer detection system," *AusWireless 06 Conference*, Sydney, Australia, 2006.
- [7] D. Deslandes and K. Wu, "Design consideration and performance analysis of substrate integrated waveguide components," *In Proc. 32nd Eur. Microw. Conf.*, vol. 2, pp. 881-884, Milan, Italy, September 2002.
- [8] Y. Zhao, J. Frigon, K. Wu, and R. Bosisio, "Numerical model of six-port and its applications," *23rd Annual Review of Progress in Applied Computational Electromagnetics (ACES)*, pp. 195-198, Verona, Italy, March 2007.
- [9] Y. Xu, L. Gerardi, Y. Zhao, M. Bozzi, L. Perregrini, K. Wu, and R. Bosisio, "Review of six-port interferometer technology," *23rd Annual Review of Progress in Applied Computational Electromagnetics (ACES)*, pp. 205-209, Verona, Italy, March 2007.
- [10] A. Koelpin, G. Vinci, B. Laemmle, D. Kissinger, and R. Weigel, "The six-port in modern society," *IEEE Microwave Magazine*, pp. 35-43, December 2010.
- [11] M. Ivanov, J. Banys, S. Rudys, and R. Grigalaitis, "Measurements of complex dielectric constant of ferroelectrics with six-port reflectometer in 80-120 frequency range," *Ferroelectrics*, vol. 367, no. 1, pp. 229-233, 2008.